CHAPTER 5

GAS PERMEATION THROUGH POLYMER BLENDS AND BLEND COMPOSITE MEMBRANES

Chapter 5

Gas Permeation through Polymer Blends and Blend Composite Membranes

5.1. Introduction

In membrane technology, variety of modifications performed to achieve better performance for mass transport process. It is very advanced technology applicable in the gas separation and filtration as it provides energy efficient processing. Membrane modification by blending of two different polymeric materials is the simplest way to modify membrane structure. In blend structure of more than one polymer, the developed composition having new chemical bonds results in different chemical and physical properties rather than origin polymers. The applications of nanocomposite materials in the membrane technology comprise high aspect ratio nanoparticles immerging in great interest, improve membrane separation and purification technology. However, numbers of research publications provide information regraded to membrane modification by blending and composite, enhancing membrane physical and chemical properties. Gas permeation and separation could have been better improved by development of hybrid membrane from two different polymers or the mixture of polymer material and inorganic filler but very less literature is available about the membrane material made up from inorganic nanofiller mixed with blended polymer matrix. The dispersion of silica nanoparticles in to polysulfone/polyimide blend improves CO_2 permeance and also reduces plasticization effect [1]. CNT reinforced polyvinyl amine/polyvinyl alcohol (PVAm/PVA) blend nanocomposite membrane improves CO_2/CH_4 selectivity at elevated pressure [2]. In the previous chapter, silica nanofillers compositing with polymer matrix enhance greatly the membrane performance for hydrogen permeation maintaining its selectivity. The next step is

carry forward in this chapter applying blend composite membranes for gas transport process and comparing the results with virgin membrane materials. The silica nanofillers are used in this work and their properties are mentioned in the **Chapter 2**.

It is discued in **Chapter 2**, the simplest polycarbonate and polysulfone were used to prepare blend membrane and 5 wt % silica nanofiller was dispersed in the polymer matrix. The thickness also affects permeability and transport properties. Quantitative discussion reported by Islam, the morphological changes as specially the film thickness affect gas permebilty in different ways as some favour the transport of flux or some hinder it. To determine the effect of thickness, some flux models can be applied as per the material used in membrane preparation [1]. Moreover, the fractional free volume depeding on the film thickness alters gas transport mechanism [3]. The material used in this work are dense polymer membranes which follows Fick's law of diffussion depending on the concentration gradient of gas flux with respect to film thickness.

The permeability of hydrogen and carbon dioxide gas was tested by using constant pressure/variable volume system developed in our laboratory. The experiment was performed at room temperature and constant 30 psi upstream pressure. Gas transport rate was obtained and permeability coefficient was calculated by this method. Oxygen transmission rate (OTR) was determined by differential pressure method at 35 ℃ constant temperature and constant 30 psi upstream pressure. The OTR was used to calculate the oxygen permeability. The gas permeability coefficients for all the given membranes were compared with reported data given in section **5.2**. Section **5.3** describes other analytic characterizations such as SEM, DSC and DMA performed to study the membrane morphology and thermal properties due to blending and dispersing nanofillers in the blend polymer matrix. The selectivity of gas pairs such as H_2/CO_2, H_2/O_2 and CO_2/O_2 was also studied for separation applications given in the section **5.4**. The outcomes of the proposed work of this chapter are summarized in the section **5.5**.

5.2. Effect of blend composites on gas transport parameters

Polymer materials used in this work are glassy polymers and both polycarbonate and polysulfone having bisphenol-A, a common ring structure in their repeating unit. PSF has also an additional ring structure and additional $-SO_2$ group in its repeating unit. The blending of these two polymers can form some additional new bonds which may affect the gas transport properties [4]. Gas permeability test performed for membranes varies from pure to blend and from blend to blend composite materials. As the materials being the class of glassy polymers follow solution diffusion mechanism under a driving force i.e. pressure gradient. In a constant pressure/variable volume system first of all the rate of gas transported through the membrane was determined at 30 psi operating pressure and at room temperature using the setup described in the **Figure 2.5** of **Chapter 2**. Gas permeability coefficient was calculated using equations **2.2** and **2.3** given in the **Chapter 2.**

5.2.1. Study of hydrogen transport

(a) Hydrogen flux across the membrane

It has been explained in **Chapter 3** that hydrogen gives faster transmission rate due to smaller kinetic diameter through the membrane compared to that of larger kinetic diameter gasses. The rate of hydrogen gas flux through the given membranes is plotted as shown in the **Figure 5.1(a)** and **5.1(b)**. Statistical analysis was performed after the downstream flow rate reaches to steady state linear approach. Hydrogen having faster permeation even at low upstream pressure, steady state is not found through any of the tested membrane. Both the figures indicate that there is raise in Hg slug height as the permeated H_2 gas flux through the membrane pushes it upward in the flow meter with increasing time. The slope of mercury height with respect to time is given in the **Table 5.1** for H_2 and CO_2. It is observed from the **Figure 5.1 (a)** that the filler content in the PC and PSF

matrix supports the flow of hydrogen gas flux as it gives faster transport rate than that of virgin polymer membranes. Consequently, the slope increases from 1.66 x 10^{-3} cm/s to 2.55 x 10^{-3} cm/s for pure PC and PC/SiO$_2$ membranes respectively. Similarly the slope increases from 1.67 x 10^{-3} cm/s to 3.20 x 10^{-3} cm/s for pure PSF and PSF/SiO$_2$ membranes respectively. In pure PC and PSF membrane the gas flux gains the mercury height up to 6 cm within 4000 seconds, whereas the filler content gains the mercury height more than 10 cm within same duration. The PSF/SiO$_2$ gives highest rate of hydrogen transport.

It is clear from **Figure 5.1 (b)** the blending of 20 wt % polysulfone with the polycarbonate do not affect the transport rate giving nearly same slope of mercury height with respect to time. Even the same blending ratio with 5 wt % SiO$_2$ nanofillers does not promote the transport rate. The PC:PSF = 80:20 (PC$_{80}$/PSF$_{20}$) blend and its composite form reduces the transport rate compared to neat polymer membranes as given the **Table 5.1**. Both these membranes raise mercury slug height up to 6 cm during same time interval. The membrane geometry such as exposed area and film thickness also affect the transport rate as it may be promoted or hindered. As the amount of PSF increased up to 40 wt % in PC/PSF blending, the H$_2$ transport rate has increased resulting gain in the mercury height up to 10 cm in 4000 seconds. The same rate can be observed by the addition of fillers to the same blending ration. Thus PC$_{60}$/PSF$_{40}$ and PC$_{60}$-PSF$_{40}$/SiO$_2$ fasters the transport rate of hydrogen. Hence, the filler incorporation in the blend polymer matrix shows same result such as their blend polymer membrane without dispersion of nanofillers. Comparing the H$_2$ transport rates for all the membranes, nanofillers dispersed in the pure polymer matrix possess better H$_2$ flux and hence penetration quality.
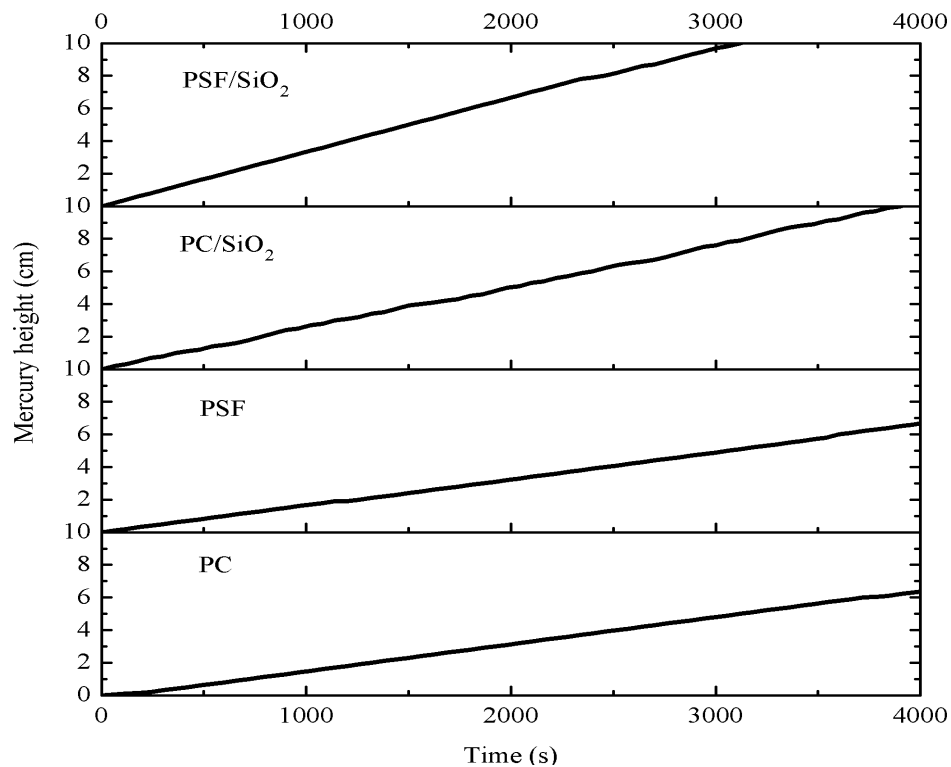
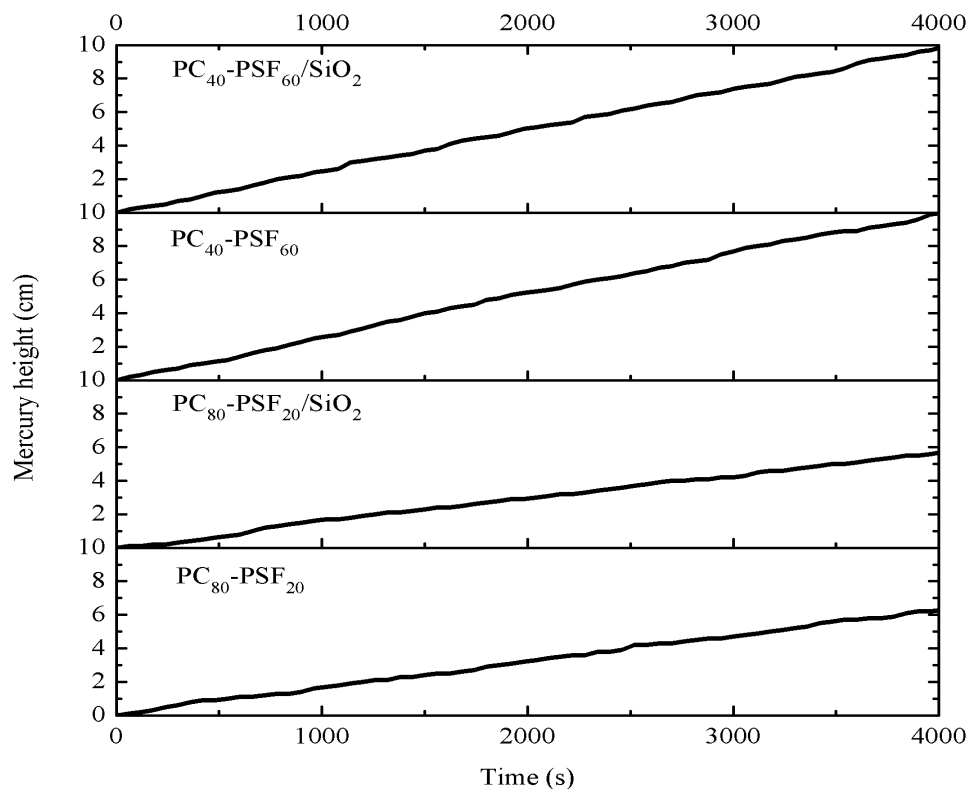**Figure 5.1 (a)** H_2 transport rate for pure and composite membranes

Figure 5.1 (b) H_2 rate for polymer blends and blend composites

93

Table 5.1 Slope of mercury height versus time for H_2 and CO_2

Material	dh/dt (cm/s) $\times$ 10^{-3}	
	H_2	CO_2
PC	1.66	1.04
PSF	1.67	1.66
PC/SiO$_2$	2.55	1.56
PSF/SiO$_2$	3.20	1.67
PC$_{80}$-PSF$_{20}$	1.52	1.18
PC$_{80}$-PSF$_{20}$/SiO$_2$	1.40	1.05
PC$_{40}$-PSF$_{60}$	2.48	1.92
PC$_{40}$-PSF$_{60}$/SiO$_2$	2.45	1.66

(b) Permeability of hydrogen

As explained in previous section, H_2 being smaller molecule rather than the rest of gases, it can easily permeate upon some operating pressure even through the dense structure. The modification in the membrane material facilitates favourable transport routes and enhances their permeation parameter. It is reported that, membrane modification by blending has promoted hydrogen permeation in varieties of materials. PC and PSF blend membrane have been improved the permeability of hydrogen gas. Moreover, the incorporation of nanofillers in the polymer matrix have enhanced hydrogen permeation likened the virgin polymer membrane. The permeability sequence differs compared to the diffused gas flux rate as the thickness and exposed area are also taken in to account. **Figure 5.2** represents permeability versus material composition of the pure and modified membranes. It is observed that as the PSF content increases in PC, hydrogen permeability decreases in small amount. This is somewhat reversed blending ratios as per the referenced data which provide the information about the enhancement of the gas permeation by increasing PC content in the PSF matrix [4]. The permeability is continuously promoted by the PC/SiO$_2$ and PSF/SiO$_2$ relative to

other compositions. The mechanism for the drastic gain in the hydrogen permeability due to presence of nanofillers in to single polymer matrix has been explained in the in **Chapter 4** and the other references provide additional information supporting the description given in the previous chapter [5, 6]. Hydrogen permeation become larger for SiO_2 doped PC, whereas it becomes more than thrice value for PSF/SiO_2 relative to PSF membrane. This represents the degree of agglomeration formed within the PSF matrix. Due to poor polymer/inorganic filler contact, tiny interface voids are developed which can be presumed to become the major cause for permeation as the gas molecules prefer less resistance path and by-pass through it instead of passing through the pores in the polymer matrix.
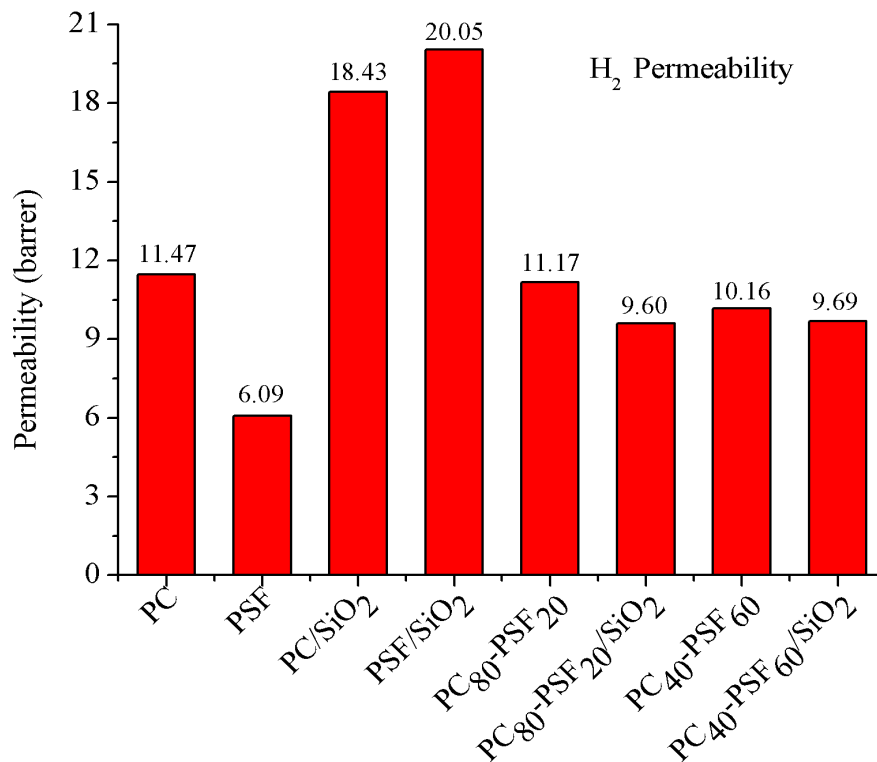

Figure 5.2 H_2 Permeability at room temperature and 30 psi feed pressure

Further modification provides change in hydrogen permeability value for blend composite membranes. Due to the filler content in the polymer blend matrix, H_2 permeation becomes smaller than their respected blend ratios. Rather to gain in

the permeation by means of the fillers it becomes hinder. The mechanism (nanogape hypothesis) explained in the previous chapter for the PNC membrane changes for H_2 permeation. In the Maxwell model, permeability decreases due to strong adhesion of filler surface in to the polymer volume. But in this case, in the blend composite membrane, the denseness increases due to the addition of filler. As the blending already forms the polymer chain interaction and also modify the polymer structure resulting in new composition, inserting the SiO_2 fillers the available free volume is blocked. This small blockage restricts the gas molecules to diffuse through the membrane matrix. Therefore, the blend composite membranes are not suitable for hydrogen permeation even than the original PC membrane.

5.2.2. Study of carbon dioxide transport

(a) Carbon dioxide flux across the membrane

Carbon dioxide transmission via pure polymer membranes, PNCs and blend composites is plotted in the **Figures 5.3 (a)** and **5.3 (b)**. Figures show, for all the membranes the occurrence of steady state time lag can be clearly observed. Being larger molecule as compared to H_2, carbon dioxide takes a small time interval to diffuse through the membrane. After the diffusion process, the nature of the plot becomes linear and the statistical analysis can be performed to determine the CO_2 transport parameters for further calculations only after steady state. The graphs plotted for raise in mercury slug versus time reveals the rate of CO_2 diffused through the tested films. PC gives smaller transport rate i.e 1.04×10^{-3} cm/s and the highest rate i.e. 1.92×10^{-3} cm/s can observed in PC_{40}-PSF_{60} as shown in **Table 5.1**. The blend ratio PC_{80}-PSF_{20} also give smaller slope value such as pure PC membrane i.e. 1.05×10^{-3} cm/s. The slopes for PSF, PC/SiO_2, PSF/SiO_2 and PC_{40}-PSF_{60}/SiO_2 are nearly same and for PC_{80}/PSF_{20} blend ratios it reduces as for pure PC. The slopes have been calculated after the steady state diffusion reached. **Table 5.2** provides time lag, diffusivity and solubility information for the material

compositions. CO_2 possess time lag value up to 700 seconds for all the membranes accept PC as it takes more time up to 1366 seconds to diffuse through the material. The difference in the time lag may be attributed to the chemical composition of the materials and also the modification formed due to the blending and dispersion of nanofillers. As the diffusivity is a time lag and film thickness dependent parameter, PSF/SiO_2 provides highest diffusion of CO_2 gas flux. Furthermore, PC/SiO_2 and PC_{80}/PSF_{20} for both blend and blend composites provide better diffusion relative to other membrane compositions. Being polar molecule, the interaction of CO_2 with the polar groups of PC changes the packing density of the membrane. This may have affected the diffusion of gas flux. The modified membranes facilitate transport routes which in turns gain in the diffusion coefficient. It can be identified that the smallest time lag provides faster diffusion of gas molecules.
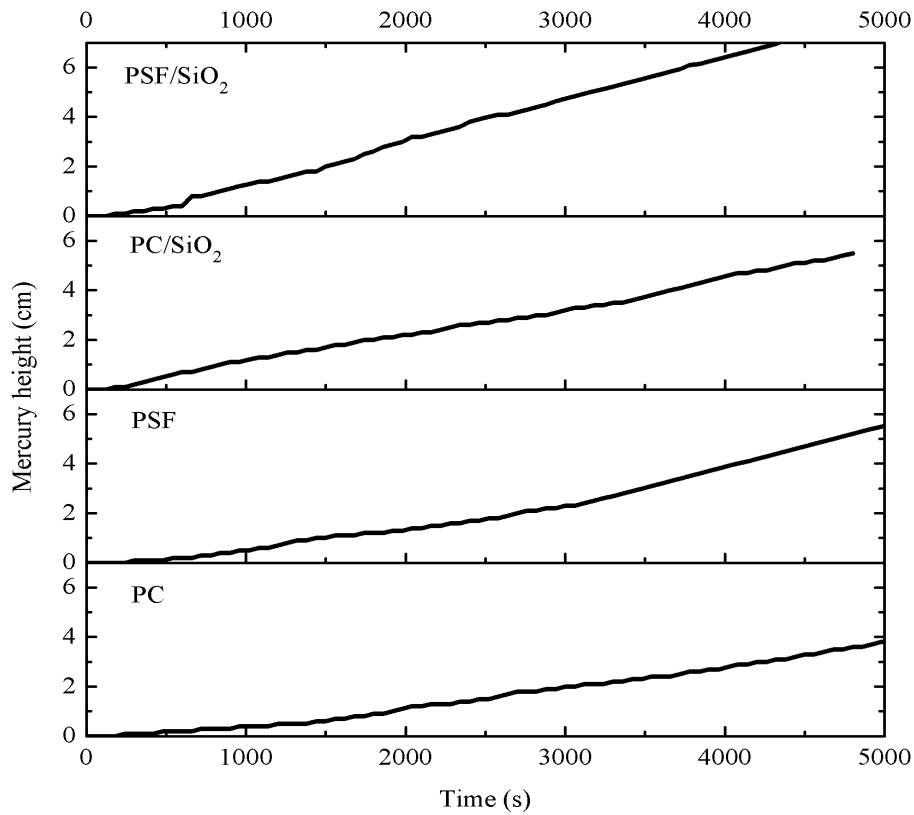

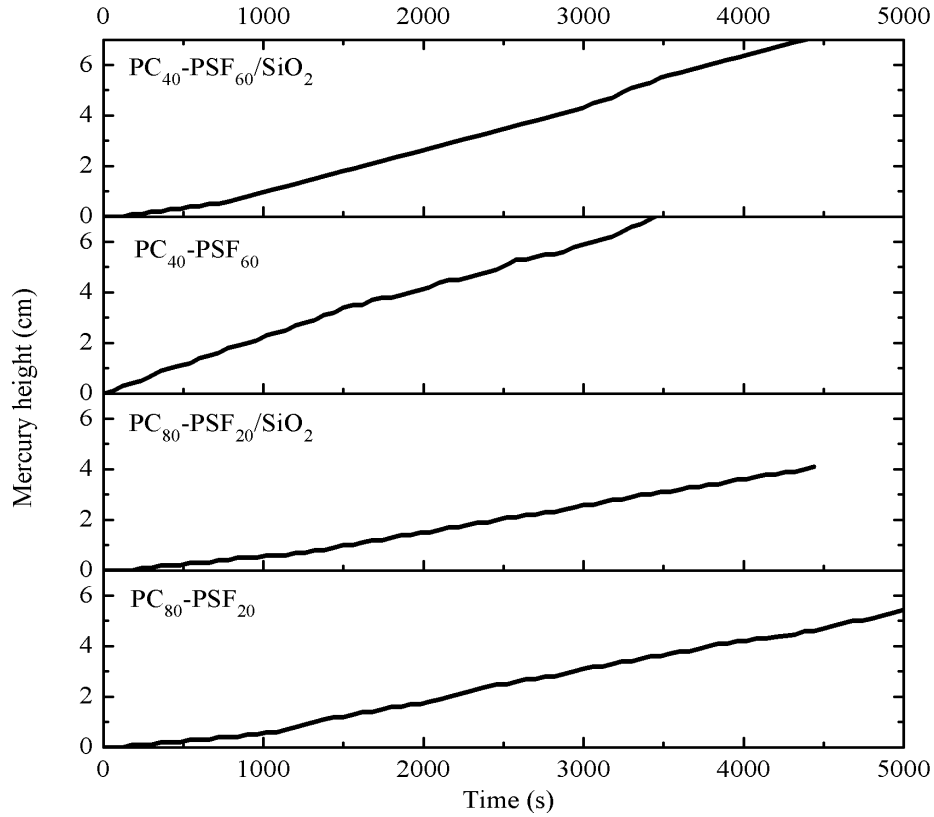**Figure 5.3 (a)** CO_2 transport rate for pure and composite membranes

Figure 5.3 (b) CO_2 transport rate for polymer blends and blend composites

Table 5.2 Carbon dioxide time lag, diffusivity and solubility

Material	Time lag (s)	$D \times 10^{-9}$ (cm^2/s)	$S \times 10^{-1}$ cm^3(STP)/cm^{3}cmHg)
PC	1366	2.99	2.46
PSF	450	2.22	2.66
PC/SiO$_2$	704	5.59	2.02
PSF/SiO$_2$	395	6.89	1.52
PC$_{80}$-PSF$_{20}$	610	5.63	1.54
PC$_{80}$-PSF$_{20}$/SiO$_2$	606	5.67	1.27
PC$_{40}$-PSF$_{60}$	450	2.86	2.75
PC$_{40}$-PSF$_{60}$/SiO$_2$	525	2.30	2.87

(b) Permeability of carbon dioxide

Carbon dioxide permeability from the different membrane compositions is given in the **Figure 5.4**. CO_2 permeability obtained by the system for pure polymer membranes matches to the reported value [5]. It was observed that the permeability obtained for PNCs has larger value compared to that of pure and blend membranes as the same hypothesis explained in the **Chapter 4**. It was observed, the blending reduces the hydrogen permeability whereas in the case of carbon dioxide, it gains due to blending effect. This may be due to the CO_2 bipolar interactions with the material composition. For the blend composite materials, it shows same trade as per the hydrogen permeation through it. CO_2 permeability also depends on its diffusivity and solubility parameters which depend on the polymer-penetrant interaction.
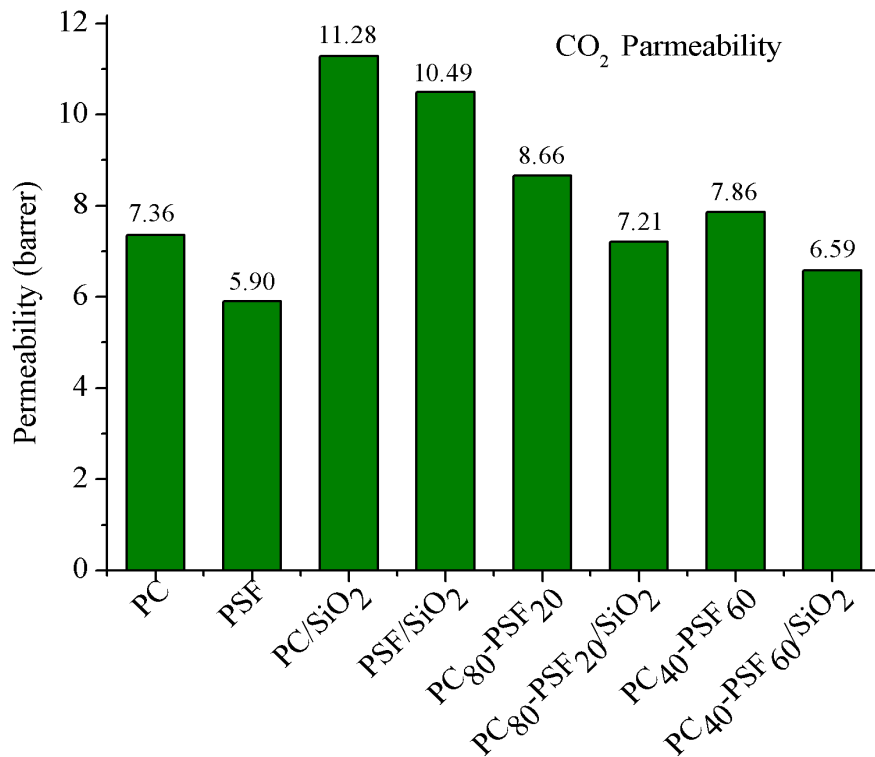

Figure 5.4 CO_2 permeability at room temperature and 30 psi feed pressure

It is reported that in the case of PC-CO_2, due to dipolar interaction gas diffusion occurs which is responsible key factor for penetration of CO_2 gas

molecules [7, 8]. It is described in **Chapter 3** that, due to the penetrant gas mixing with the polymer chain segments solubility varies with the material composition. The solubility coefficient is also calculated by permeability-diffusivity relation using equation **1.2** mentioned in the **Chapter 1**. As CO_2 is polar molecule, it is soluble in the polymer matrix having polar functional groups. Therefore, condensation occurs between the carbon dioxide and the polymer composition which will affect the solubility parameter. For PSF/SiO_2, $PC_{80}-PSF_{20}$ and $PC_{80}-PSF_{20}/SiO_2$ solubility reduces as shown in **Table 5.2** due to poor mixing of gaseous penetrant with the polymer mobile segments which alters the CO_2 permeation in distinct way.

5.2.3. Study of oxygen transport

(a) Oxygen Transmission Rate (OTR)

Oxygen transmission rate of the present series of membranes was characterized by differential pressure method using i-Gastra 7100 Gas permeability tester by Labthink, China. **Table 5.3** represents the OTR values for respective membranes. Unfortunately, OTR for pure PSF could not obtained as the material was in damaged condition at the time of testing. The highest OTR value has been observed for pure $PC_{40}-PSF_{60}$ is 3.99×10^{-7} and for pure PC membrane it shows lowest value i.e. 0.66×10^{-7}. For the other membranes, the internal structure is modified which may affect the flow of oxygen gas molecules resulting in the reduction of transmission rate. OTR for $PC_{80}-PSF_{20}$ reduces as the PC wt% is more as comparted to PSF. For rest of the membranes it decreases due to gain in other composition amounts than PC. For $PC_{80}-PSF_{20}/SiO_2$ and PC/SiO_2 OTR value is 2.96×10^{-7} which is almost 3×10^{-7} but as the PSF amount is increased up to 60 wt% and decreased PC amount up to 40 wt%, it shows further reduction in the OTR. The result indicates that if the other compositions are mixed with PC, the resulted material demotes the OTR. The permeability of H_2 and CO_2 for PC/SiO_2 (5wt% filler content) membrane is matched with the reported values for same

composition (10wt% filler content) [5]. For PSF/SiO$_2$ permeably of all the three gasses increases in vast amount compared to the values obtained by Ahn et al. with same filler content [9].

Table 5.3 Oxygen transmission rate determined by gas permeability tester

Material	OTR cm^3(STP)/cm^2·s·cmHg
PC	0.66E-07
PSF	--
PC/SiO$_2$	2.96E-07
PSF/SiO$_2$	2.90E-07
PC$_{80}$-PSF$_{20}$	2.36E-07
PC$_{80}$-PSF$_{20}$/SiO$_2$	3.01E-07
PC$_{40}$-PSF$_{60}$	3.99E-07
PC$_{40}$-PSF$_{60}$/SiO$_2$	3.60E-07

(b) Permeability of oxygen

Oxygen permeability was determined from the OTR values which do not follow the same sequence such as its transmission rate values as the most important parameter membrane thickness is introduced for the calculation of permeability coefficient. Membrane thickness is an important factor in gas permeability calculation because the gas permeation is thickness dependent parameter [10]. The oxygen permeability of proposed membrane is represented by the graph shown in the **Figure 5.5**.

It was observed that there is drastic change in the permeability due to the incorporation of filler particles. For PC/SiO$_2$ it enhances more than four times the original membrane. It was also observed that not only for PC but also for PSF/SiO$_2$ the permeability increases by larger value relative to that of PSF. By introducing the blending effect in PC with PSF in 80:40 wt % ratios, permeability

for PC increases and it further gains as the PSF content increases up to 60 wt %. This shows somewhat reversed manner compared to the permeability of H_2 and CO_2 which reduces for gain in the PSF content with PC. This may be due to the different environmental conditions and system used for the gas permeation testing. The filler content in the blend matrix follow the same manner as per their effect in H_2 and CO_2 permeation. It reduces O_2 permeation relative to their respected blend membrane. The changes may occur due to the difference in size and shape of oxygen molecules relative to H_2 and CO_2. The permeability of H_2 and CO_2 for PC/SiO_2 (5 wt% filler content) membrane is matched with the reported values for same composition (10 wt% filler content) [5]. For PSF/SiO_2 permeably of all three gasses increases in vast amount compared to the values obtained by Ahn et al. with same filler content [9].
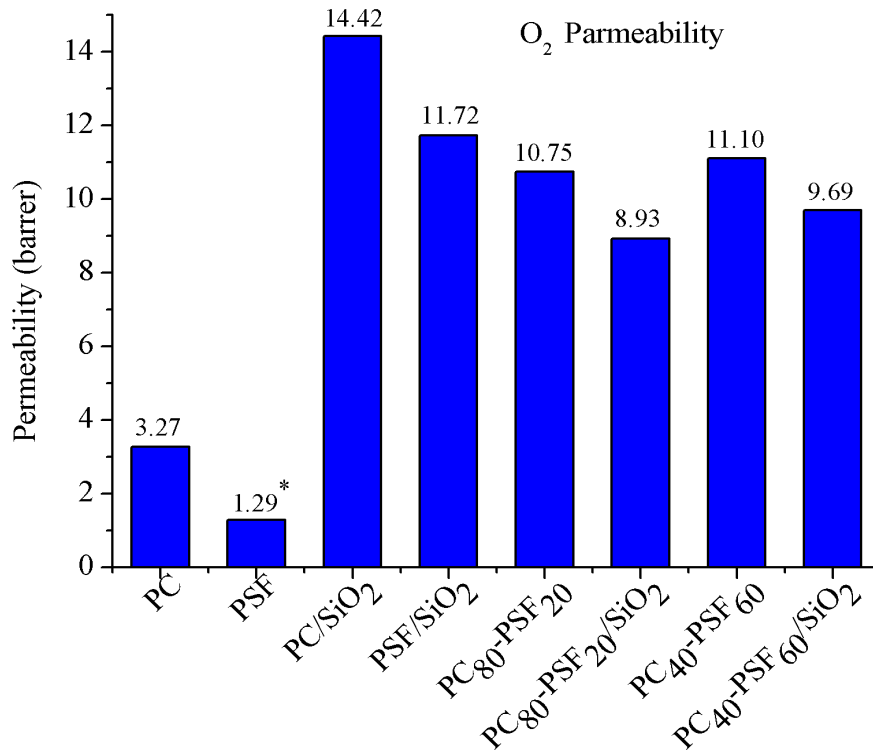

Figure 5.5 Permeability of O_2 tested at 35 ℃ temperature and 30 psi feed pressure

(* Used from reference [9])

5.3. Other analytical characterizations

5.3.1. Membrane appearance

Figure 5.6 (a) and **5.6 (b)** shows various images of the developed membranes using solution cast method. The images were captured by Samsung SM-G615FU camera of 13-megapixels with 4128 x 3096 image resolution by adjusting 3.71 mm focal length. It can be observed that the pure polymer membranes shows higher transparency compared to blend and composite membranes. Agglomeration at some extent can be viewed in PC/SiO$_2$ membrane and the blend membrane images looks blurred compared to that of unmodified membranes. The doping of nanofillers in to the blend matrix increases the blurring effect.

Figure 5.6 (a) Optical micrograph of pure and SiO$_2$ doped polymer membranes.

Figure 5.6 (b) Optical micrograph of blend and SiO_2 doped blend membranes.

5.3.2. Scanning Electron Microscopy (SEM)

The change in the morphology with filler content has been explained in the previous chapter in the section **4.4.1** described by **Figure 4.7**. The SEM image of polymer nanocomposite (PC/SiO_2) membrane is shown in **Figure 5.7** which shows the dispersion of SiO_2 in polymer matrix. The SEM image was obtained for this sample as all the other membranes contain same filler amount. It is observed that the silica content produces roughness on the membrane surface. The filler agglomeration is identified from the SEM image. Pure polymer membrane shows dense structure as reported by Idris et.al. [11]. The same filler content in PSF matrix changes the surface morphology as per the reported data [9, 12].
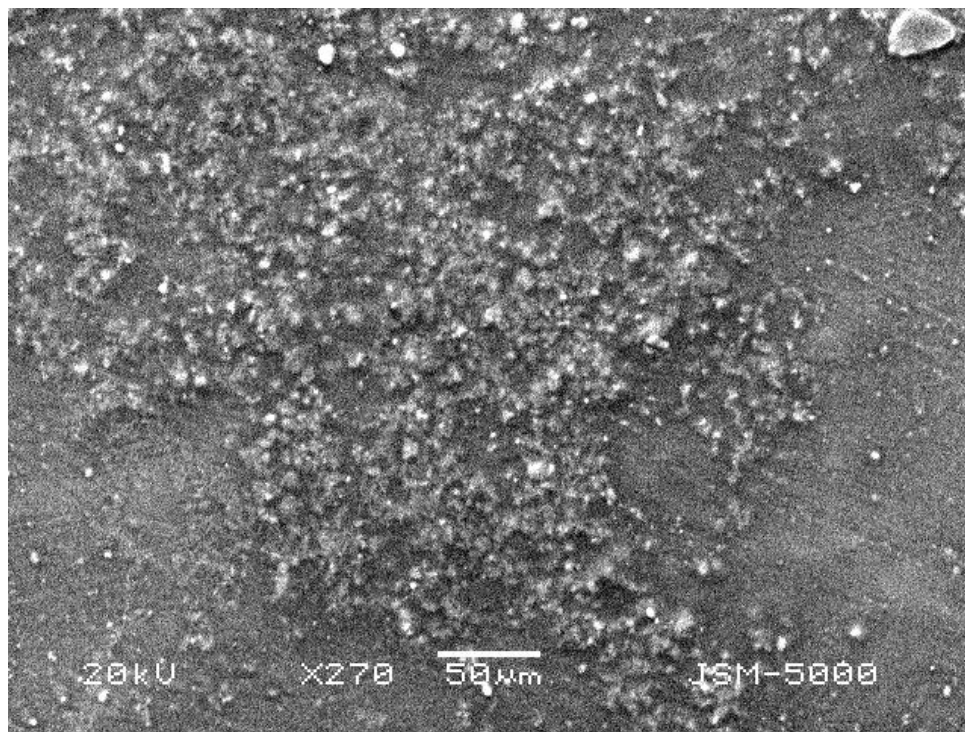
Figure 5.7 SEM image of PC/SiO$_2$ mixed matrix membrane

5.3.3. Differential Scanning Calorimetry (DSC)

Figure 5.8 (a) to **5.8 (d)** indicates the nature of differential scanning calorimetry (DSC) thermogram for blend and composite membrane. The glass transition temperatures (T$_g$) along with the heat capacity are given in **Table 5.4**. The materials are used in the form of blend and blend composites. The miscibility of composites is indicated by variation in T$_g$ value. The perfect miscible polymer matrix gives a single T$_g$ value as it shows homogeneous distribution of polymer chain segments. In a phase separated blend, two or more transition temperatures occur which can be avoided by using a compatibility agent. It is observed that the T$_g$ show distinct value for all the materials which is a good indication of mixing of different compositions. The reported T$_g$ for pure PC and PSF are 144.36 ℃ [11] and 178.55 ℃ [13] respectively. Although having same phenyl ring structure and functional groups, PSF having additional –SO$_2$ connector group, it raises in glass transition temperature compared to that of PC [14]. The T$_g$ of blend membrane lies

between those of individual polymers. It is also observed that there is gain in the transition temperature with the silica nanoparticles loading by 0.63 °C in PC/SiO$_2$. Subsequent stress is formed at the particle-polymer interface during the membrane casting process. The change is attributed to small rigidified region developed in the membrane matrix which promotes long range segmental mobility of polymer chains and hence increase in T$_g$ value. In PSF/SiO$_2$ T$_g$ gains compared to PC/SiO$_2$ which indicates more segmental chain mobility [13, 15, 16]. The heat capacity also varies with change in compositions. It is highest for blend polymer and filler reduces the ΔC_p.
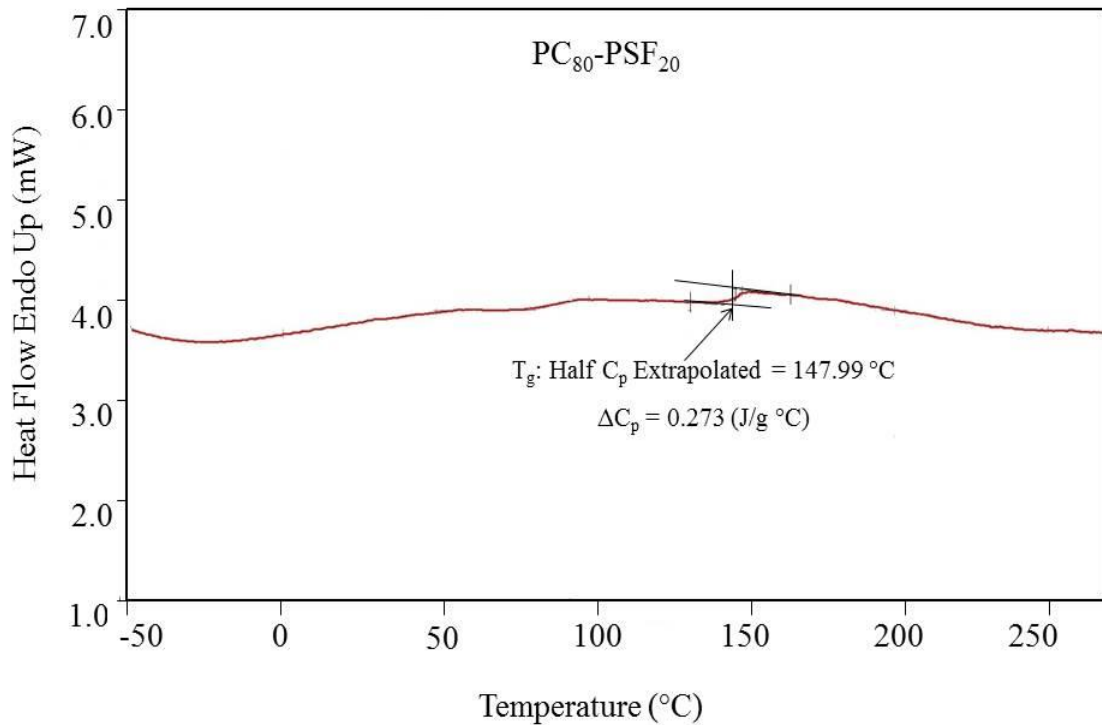

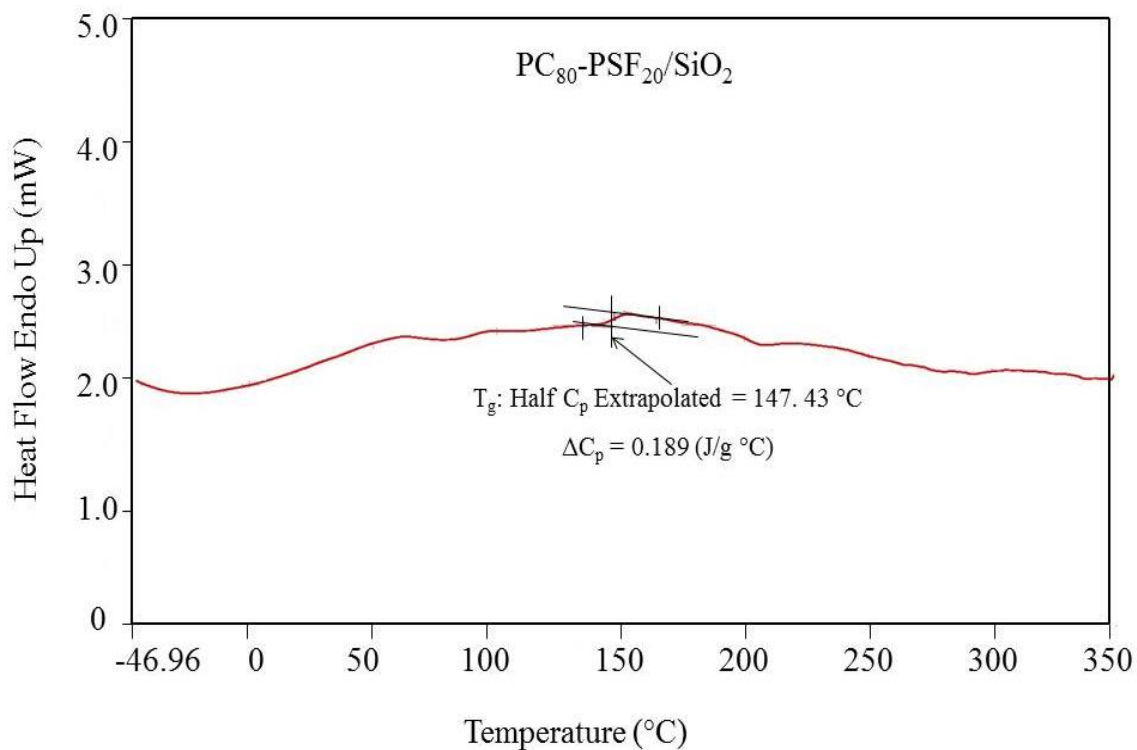**Figure 5.8 (a)** Heat flow versus temperature for PC$_{80}$-PSf$_{20}$

Figure 5.8 (b) Heat flow versus temperature for $PC_{80}PSF_{20}/SiO_2$
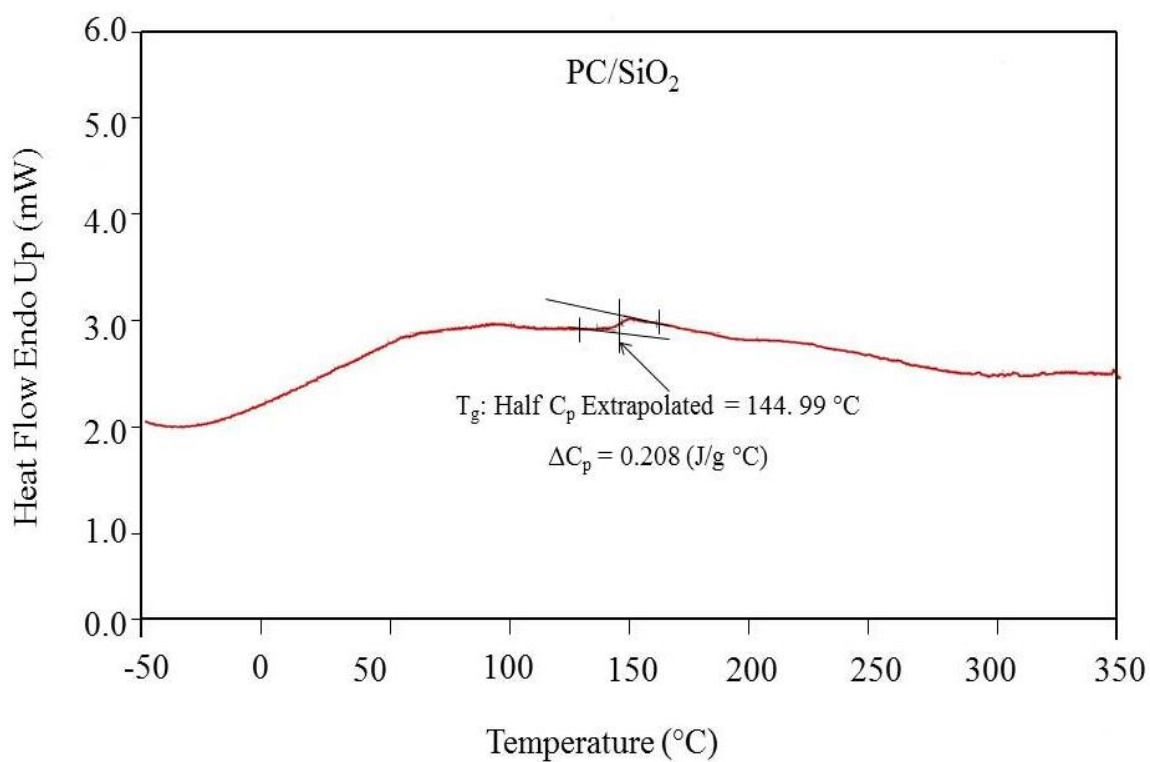

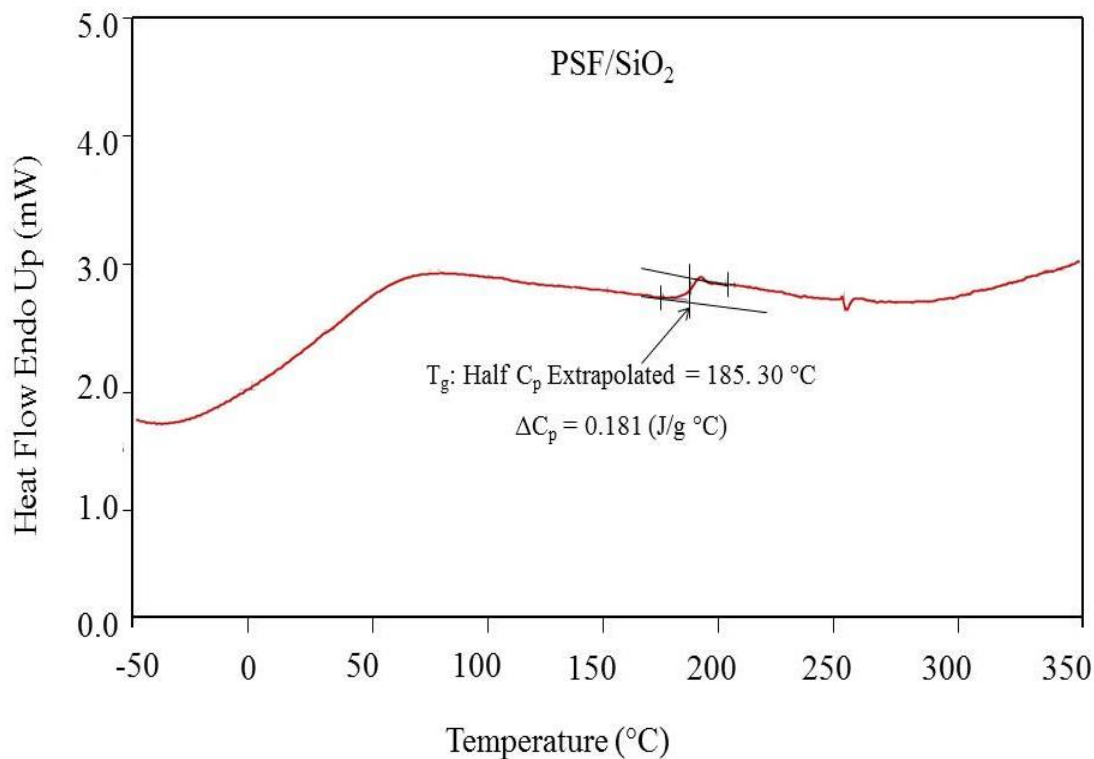**Figure 5.8 (c)** Heat flow versus temperature for PC/SiO_2

Figure 5.8 (d) Heat flow versus temperature for PSF/SiO$_2$

Table 5.4 Glass transition temperature and specific heat of blend and composite
membranes

Materials	DSC	
	T_g (ºC)	ΔC_p (J/g ºC)
PC$_{80}$-PSF$_{20}$	147.99	0.273
PC$_{80}$PSF$_{20}$/SiO$_2$	147.43	0.189
PC/SiO$_2$	144.99	0.208
PSF/SiO$_2$	185.30	0.181

5.3.4. Dynamic Mechanical Analysis (DMA)

The analysis has been performed in temperature scan mode to study
modulus factor and damping behaviour. At the high storage modulus, the material
is hard and becomes soften as the modulus decreases. The detail of geometrical
parameters of the membrane tested and environmental conditions are mentioned in

the **Chapter 2** in section **2.5.3**. Plot of modulus and damping versus temperature is shown in the **Figure 5.9 (a)** to **5.9 (d)**. The peak value of tan δ corresponds to glass transition temperature of the material is given by the solid line intersected with damping curve. The glass transition temperature at damping peak is compared with T_g value obtained from DSC analysis. There is slight difference in the glass transition temperatures obtained from both analyses. As the T_g is not a single value, it is a range of behaviour of material but the average unit number is considered as given in literature. In DSC and DMA, the experiment is performed by different processes and at different frequencies. Therefore, a slight variation has been observed in T_g. For PC/SiO_2 mixed matrix membrane, T_g differs nearly by 10 ºC by both characterizations in the presented study whereas in the reported data T_g obtained from DSC matches with the T_g obtained from DMA in the proposed work with the same silica content [11]. This may be attributed to different environmental conditions during the membrane casting process or due to operating conditions during characterization.

Comparing tan δ for the compositions, PC/SiO_2 shows highest value of damping as given in **Table 5.5**. As damping is the ratio of loss modulus to storage modulus, it gives the energy dissipated in the polymer matrix. Polymer blend possess lower energy dissipation whereas filler content affect the damping factor. The highest energy loss is given by PC/SiO_2 nanofillers. It is observed by membrane appearance, this composition shows more agglomeration relative to other membrane materials. Thus poor adhesion may cause to gain the damping factor. Membrane compositions PC_{80}-PSF_{20} and PC_{80}-PSF_{20}/SiO_2 shows two different transitions for damping plot due to interaction of chain segments by polymer blending. This modification cause local chain motion due to repeated units [17].
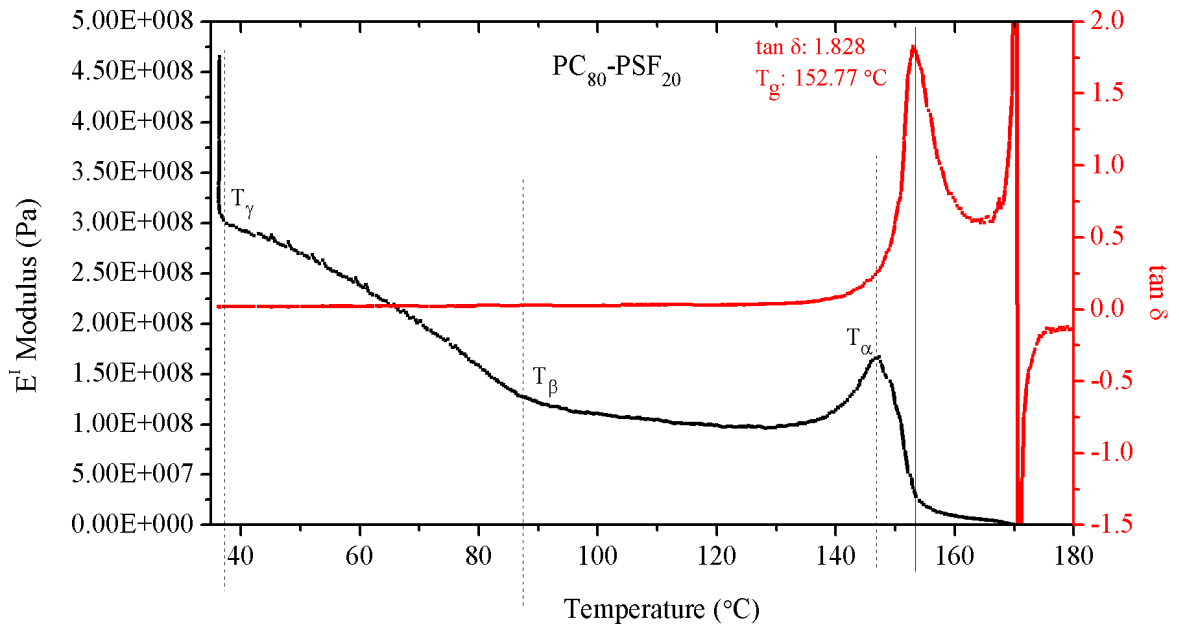
Figure 5.9 (a) Temperature scan of modulus and damping for PC$_{80}$-PSf$_{20}$

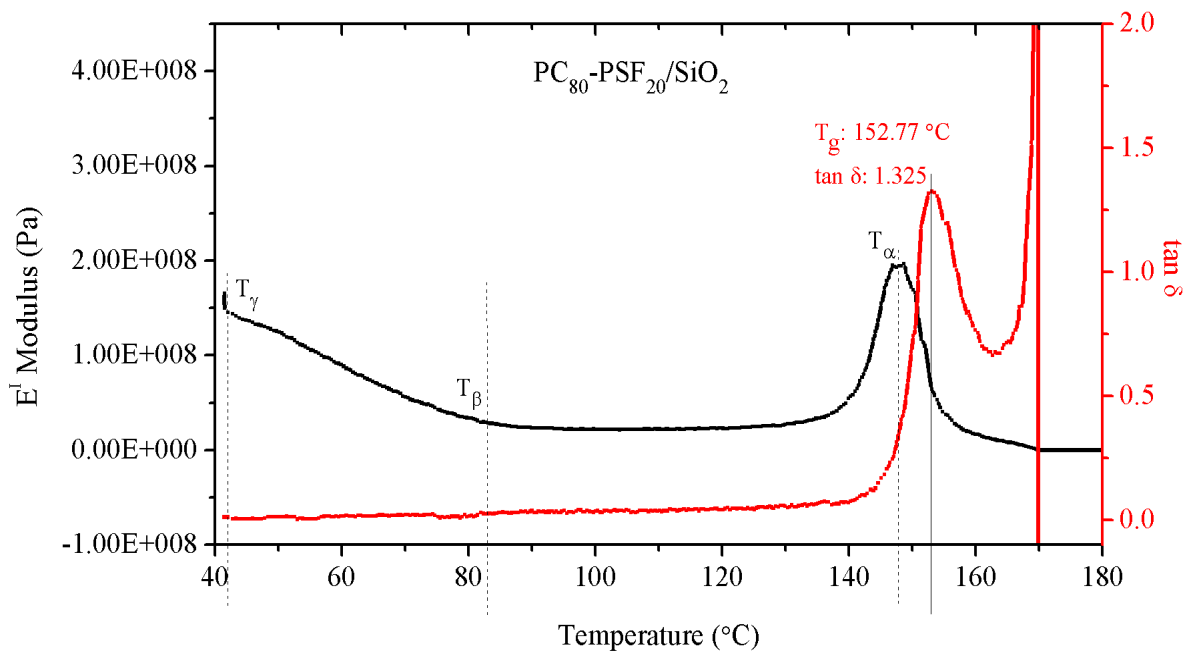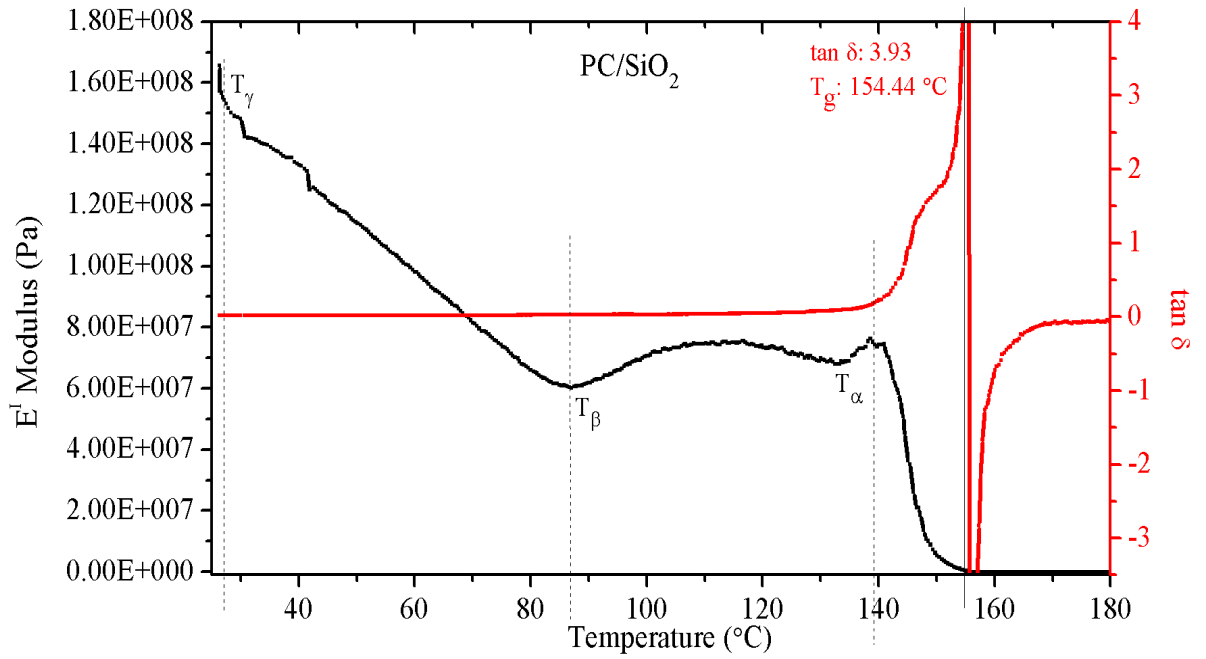**Figure 5.9 (b)** Temperature scan of modulus and damping for PC$_{80}$PSF$_{20}$/SiO$_2$

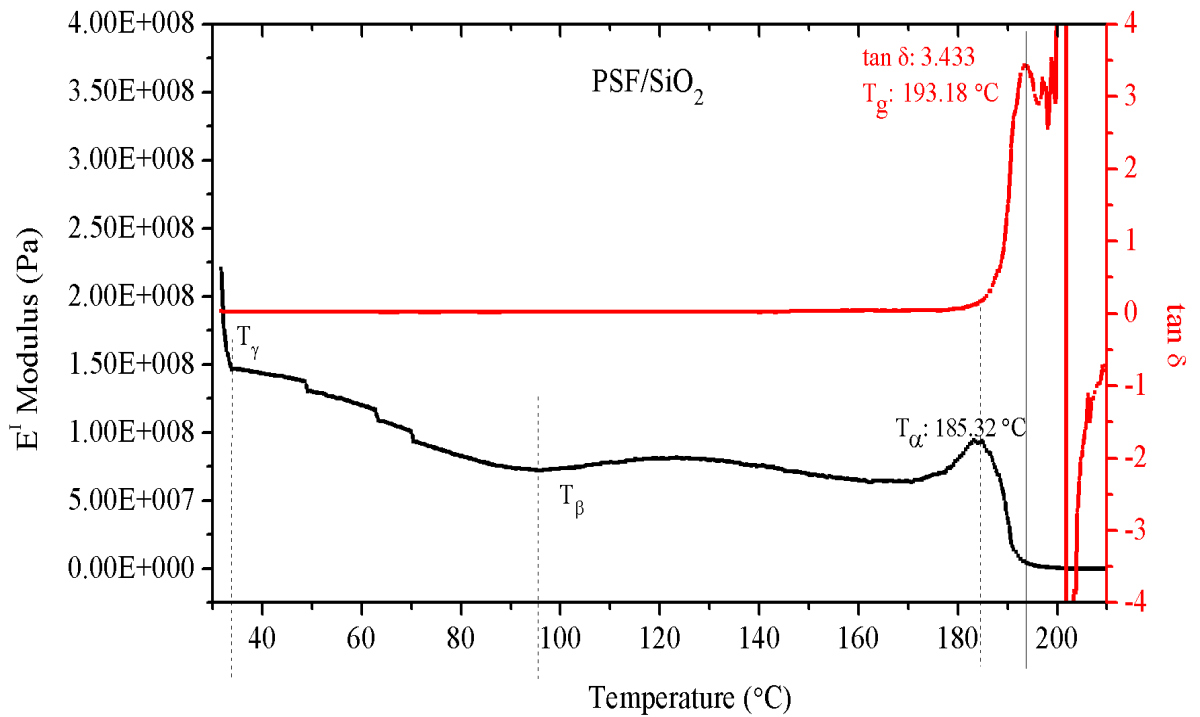**Figure 5.9 (c)** Temperature scan of modulus and damping for PC/SiO$_2$

Figure 5.9 (d) Temperature scan of modulus and damping for PSF/SiO$_2$

111

As shown in the plots the dashed lines intersected with the modulus curve gives different transition temperatures. The modulus data and damping factor are given in the **Table 5.5**. The highest modulus is 0.46 GPa obtained for polymer blend mixture. The filler content reduces the storage modulus. The incorporation of filler content which is blocked inside the blend crosslinking network results in rigid volume structure. Therefore, PC_{80}-PSF_{20}/SiO_2 shows lowest modulus value as E^I is associated to the stiffness of membrane material. The blending possesses highest modulus due to flexible chain orientation [18]. The dashed lines interacted with the modulus curve shows transition temperatures. The T_γ transition occurs rapidly as the temperature starts gaining due to local chain movements and band stretching. The region between T_γ and T_β is related to the toughness and motion of atoms in the main chain. Beyond T_β transition the phase change occurs and the composition moves towards glass transition temperature which is often denoted by T_α [19].

Table 5.5 Glass transition temperature, tan δ and modulus of blend and composite membranes

Materials	DMA		
	T_g (ºC)	tan δ	E^I (GPa)
PC_{80}-PSF_{20}	152.77	1.828	0.46
$PC_{80}PSF_{20}/SiO_2$	152.77	1.325	0.16
PC/SiO_2	154.44	3.937	0.17
PSF/SiO_2	193.18	3.433	0.22

5.4. Effect of blend composites on selectivity

Table 5.6 shows the selectivity for pure, blend and blend composite membranes for H_2/CO_2, H_2/O_2 and CO_2/O_2 gas pairs. The highest selectivity is obtained for H_2/O_2 and CO_2/O_2 gas pairs for pure polymeric membranes. For H_2/CO_2 gas pair, PSF/SiO_2 and PC/SiO_2 MMMs gives better performance relative

to other membrane materials. Hydrogen separation from carbon dioxide reduces due to blending effect. But the filler content in single polymer matrix shows improvement in the selectivity relative to blend composite membranes. Both polymer blends gives same separation factor of H_2/CO_2 whereas silica content in PC_{40}-PSF_{60} blend ratio performs better as compared to PC_{80}-PSF_{20}/SiO_2. The selectivity of H_2 over CO_2 for PSF/SiO_2 gains 91 % compared to that of pure PSF membrane which directs towards the trade-off upper bound limit. It is observed that relative to pure PSF materials all the membranes gives better separation factor for H_2 over CO_2. The separation of hydrogen from oxygen favours for pure polymeric membranes. The lowest selectivity for this gas pair is shown by PC_{40}-PSF_{60} blend ratio although its permeability for hydrogen is not the highest value. For CO_2/O_2 gas pair, the filler content does not affect the selectivity by PC_{80}/PSF_{20} blend ratio.

Table 5.6 Selectivity of H_2/CO_2, H_2/O_2 and CO_2/O_2

Material	H_2/CO_2	H_2/O_2	CO_2/O_2
PC	1.56	3.50	2.25
PSF	1.0	4.72	4.58
PC/SiO_2	1.63	1.28	0.78
PSF/SiO_2	1.91	1.71	0.90
PC_{80}/PSF_{20}	1.29	1.04	0.81
PC_{80}-PSF_{20}/SiO_2	1.33	1.07	0.81
PC_{40}-PSF_{60}	1.29	0.92	0.71
PC_{40}-PSF_{60}/SiO_2	1.47	1	0.68

The surface morphology also affects the selectivity as it is higher for pure polymer composite membranes that show surface roughness as discussed in section **5.3.2**. The interaction of gas molecules differs with dense and rough surface at the exposure time upon particular feed pressure which affects

permeation of gas molecules of different kinetic diameters. The change in glass T_g also affects the selectivity due to the segmental motion of polymer which allows to pass particular gas species depending on the shape and size of gas molecules.

5.5. Summary

Gas transportation through the synthesized pure membranes gives comparative results from literature values. The filler incorporation in the pure polymer matrix facilitates more transport route for H_2, CO_2 and O_2 gas molecules. All these experimental gasses show highest gas transport rate and permeability in the PNC membranes. The gas transportation in the modified membrane increase compared to that of neat membranes. Having smallest kinetic diameter, hydrogen gas diffuses faster relative to the other gasses. The nanofillers produce enough space inside the polymer matrix to bypass the gas molecules under the operating conditions. Hydrogen permeation reduces for blends and blend composites while, CO_2 permeation reduces for both blend composites only relative to that of pure PC membrane. Observing the filler effect in blend matrix for O_2 gas, it does not improve the transport of gas molecules compared to the same blend ratio but improves permeability relative to pure polymer membranes. The membrane modification affects distinctly and depends on the nature of penetrant. The separation factor is also affected by the modifications. Separation factor for H_2/CO_2 is improved due to the alteration whereas it scales down for the other gas pairs. Therefore, the modified membranes can be used to separate hydrogen gas from the mixture with carbon dioxide for their effective applications. The surface morphology of the PNC membrane provides information about the effective roughness developed on the membrane surface due to nanofillers. Moreover, thermal analysis provides the information about the effect of blending and nanofillers on the T_g and heat capacity. Glass transition temperature reduces due to the alteration and hence effectively reduces the heat capacity of the membrane. The filler content increases the damping factor (tan δ) which may be affected due

to poor adhesion between SiO_2 nanofiller and the polymer network. The storage modulus reduces for nanocomposite membranes. In blending, the silica loading forms blockage within the polymer chain network up to some extends which restricts particular penetrant to bypass. The overall result concludes that the dispersion of nanofillers in the pure polymer matrix performs better as compared to that of the blend matrix particularly for gas permeation applications.

References

[1]   S. Rafiq, Z. Man, A. Maulud, N. Muhammad, S. Maitra, Separation of CO_2 from CH_4 using polysulfone/polyimide silica nanocomposite membranes, *Sep. Puri. Tech.* 90 (2012) 162–172.

[2]   L. Deng, M. Hagg, Carbon nanotube reinforced PVAm/PVA blend FSC nanocomposite membrane for CO_2/CH_4 separation, *Int. J. of Greenhouse Gas Control.* 26 (2014) 127–134.

[3]   G. Firpo, E. Angeli, L. Repetto, U. Valbusa, Permeability thickness dependence of poly-dimethylsiloxane (PDMS) Membrane, *J. Memb. Sci.* (2014) http://dx.doi.org/10.1016/j.memsci.2014.12.043.

[4]   K. Awasthi, V. Kulshreshtha, B. Tripathi, N.K. Acharya, M. Singh, Y.K. Vijay, Transport through track etched polymeric blend membrane, *Bull. Mater. Sci.* 29 (2006) 261–264.

[5]   N.K. Acharya, Temperature-dependent gas transport and its correlation with kinetic diameter in polymer nanocomposite membrane, *Bull. Mater. Sci.* 40 (2017) 537–543.

[6]   A.K. Patel, N.K. Acharya, Metal coated and nanofiller doped polycarbonate membrane for hydrogen transport, *Int. J. Hydrogen Energy*. 43 (2018) 21675–21682.

[7]   S.H. Chen, S.L. Huang, K.C. Yu, J.Y. Lai, M.T. Liang, Effect of CO_2 treated polycarbonate membranes on gas transport and sorption properties, *J. Memb. Sci.* 172 (2000) 105–112.

[8] T.A. Barbari, W.J. Koros, D.R. Paul, Gas transport in polymers based on bisphenol-A, *J. Polym. Sci. Part B Polym. Phys.* 26 (1988) 709–727.

[9] J. Ahn, W.J. Chung, I. Pinnau, M.D. Guiver, Polysulfone/silica nanoparticle mixed-matrix membranes for gas separation, *J. Memb. Sci.* 314 (2008) 123–133.

[10] M.A. Islam, H. Buschatz, Assessment of thickness-dependent gas permeability of polymer membranes, *Indian J. Chem. Tech.* 12 (2005) 88–92.

[11] A. Idris, Z. Man, A.S. Maulud, Polycarbonate/silica nanocomposite membranes: Fabrication, characterization, and performance evaluation, *J. Appl. Polym. Sci.* 134 (2017) 1–17.

[12] S.M. Momeni, M. Pakizeh, Preparation, characterization and gas permeation study of psf/mgo nanocomposite membrane, *Brazilian J. Chem. Eng.* 30 (2013) 589–597.

[13] H. Abdul Mannan, H. Mukhtar, M. Shima Shaharun, M. Roslee Othman, T. Murugesan, Polysulfone/poly(ether sulfone) blended membranes for CO_2 separation, *J. Appl. Polym. Sci.* 133 (2016) 1–9.

[14] D.R. Paul, Y.P. Yampolskii, Polymeric Gas Separation Membranes, *CRC Press Inc.*, Boca Raton Ann Arbor London Tokyo, London (1994).

[15] N.P. Patel, A.C. Miller, R.J. Spontak, Highly CO_2-permeable and -selective membranes derived from crosslinked poly(ethylene glycol) and its nanocomposites, *Adv. Funct. Mater.* 14 (2004) 699–707.

[16] T.T. Moore, W.J. Koros, Non-ideal effects in organic-inorganic materials for gas separation membranes, *J. Mol. Struct.* 739 (2005) 87–98.

[17] M. Aguilar-Vega, D.R. Paul, Gas transport properties of polycarbonates and polysulfones with aromatic substitutions on the bisphenol connector group, *J. Polym. Sci. Part B Polym. Phys.* 31 (1993) 1599–1610.

[18] A.D. Mulliken, M.C. Boyce, Mechanics of the rate-dependent elastic–plastic deformation of glassy polymers from low to high strain rates, *Int. J. Solids*

Struct. 43 (2006) 1331–1356.

[19] K.P. Menard, Dynamic mechanical analysis: A Practical Introduction, *CRC Press LLC*, (1999).